Editors' Suggestion

Theory of a Carbon-Nanotube Polarization Switch

Ken-ichi Sasaki*
NTT Basic Research Laboratories, NTT Corporation, 3-1 Morinosato Wakamiya, Atsugi, Kanagawa 243-0198, Japan

Yasuhiro Tokura
Faculty of Pure and Applied Sciences, University of Tsukuba, Tsukuba, Ibaraki 305-8571, Japan

(Received 31 October 2017; revised manuscript received 5 November 2017; published 21 March 2018)

Recently, it was suggested that the polarization dependence of light absorption to a single-walled carbon nanotube is altered by carrier doping. We specify theoretically the doping level at which the polarization anisotropy is reversed by plasmon excitation. The plasmon energy is mainly determined by the diameter of a nanotube because pseudospin makes the energy independent of the details of the band structure. We find that the effect of doping on the Coulomb interaction appears through the screened exchange energy, which can be observed as changes in the absorption peak positions. Our results strongly suggest the possibility that oriented nanotubes function as a polarization switch.

DOI: 10.1103/PhysRevApplied.9.034018

I. INTRODUCTION

A carbon nanotube (CNT) [1] absorbs light whose linear polarization is parallel to the tube's axis ($\mathbf{E}_{\parallel}$) but not when the polarization is perpendicular to it ($\mathbf{E}_{\perp}$) [2–4]. The optical anisotropy of a CNT enables oriented CNTs to function as an optical polarizer [5,6]. Recently, it was theoretically predicted that the polarization dependence is reversed by charge doping [7]; a doped CNT transmits $\mathbf{E}_{\parallel}$ and absorbs $\mathbf{E}_{\perp}$ (see Fig. 1).

The absorption of $\mathbf{E}_{\perp}$ originates from the resonant excitation of collective oscillations of electrons (plasmon), which differs entirely from the excitation of individual electrons or excitons by $\mathbf{E}_{\parallel}$ in an undoped CNT [7,8]. This theory of plasmon resonance accounts qualitatively for the anomalous absorption peaks observed experimentally in doped CNTs [9–12]. However, because the theoretical conclusion was derived using the Drude model, which takes account only the intraband electronic transitions, the exact doping and chirality [13] dependences of the absorption spectrum remain unknown.

In this paper, we elucidate these dependences by investigating the competition between intra- and interband transitions with the Kubo formula. On the basis of predicted doping and chirality dependences, we conclude that doped CNTs absorb $\mathbf{E}_{\perp}$ over frequencies ranging from infrared to visible. This expands the application range of CNT polarizers and suggests the possibility that the polarization direction of transmitted light is changed by 90° with doping rather than by spatial rotation.

This paper is organized as follows. In Sec. II, we explain the optical selection rule of CNTs. By calculating the dynamical conductivity, we show that momentum conservation and pseudospin play very essential roles in determining the possible transitions. In Sec. III, we examine absorption spectra for armchair and zigzag CNTs, which are the main result of this paper. The effect of Coulomb interaction on the absorption spectra is studied in Sec. IV. Our discussion is provided in Sec. V. The calculation details, which are necessary to reproduce the results of Secs. II and III, are given in the Appendix.

II. SELECTION RULE

A. Parallel polarization

The electronic transition caused by $\mathbf{E}_{\parallel}$ is a direct transition without a change in momentum of a photoexcited electron [2]. In the band diagram of a (10,10) armchair CNT shown in Fig. 2(a), each of the band curves plotted as a function of the wave vector along the tube's axis ($k_{\parallel}$) is an eigenstate of the momentum around

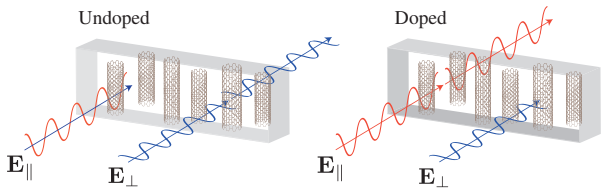

FIG. 1. Optical anisotropy of oriented CNTs. Oriented and undoped (doped) CNTs pass $\mathbf{E}_{\perp}$ ($\mathbf{E}_{\parallel}$) only. Thus, oriented CNTs function as a polarization switch.

*sasaki.kenichi@lab.ntt.co.jp

it and specified by magnetic quantum number m [14]. The two bands with linear dispersion that cross each other at $E = 0$ have vanishing m, while the other curve is degenerate ($\pm|m|$) corresponding to the clockwise and anticlockwise circumferential motions, and the magnitude $|m|$ increases with the energy $|E|$. Because the same m value appears in the conduction and valence bands symmetrically with respect to $E = 0$, there are two possible cases of direct transition: transition between the valence and conduction bands (interband transition) or within either band (intraband transition).

The doping dependence of the direct interband transition is roughly known from Fermi-Dirac statistics. When the doping level is low, e.g., $E_F = 0$ eV (undoped), the direct interband transitions denoted by M_{11} and M_{22} in Fig. 2(a) are both allowed by the Pauli exclusion principle [15,16], while when the doping level is high, e.g., $E_F = 1$ eV, M_{11} is forbidden, although M_{22} is still allowed. In Fig. 2(b), the calculated real part of the dynamical conductivity $\mathrm{Re}(\sigma_\parallel)$ shows that the M_{11} peak disappears when $E_F = 1$ eV. Meanwhile, a Drude peak corresponding to the direct intraband transition denoted by D in Fig. 2(a) develops in the zero-frequency limit of $\mathrm{Re}(\sigma_\parallel)$. The peak intensity increases with doping because the density of states at E_F increases with doping. The disappearance of the M_{11} peak and enhancement of the Drude peak are evidence of high doping that is provided by the absorption spectra of $\mathbf{E}_\parallel$.

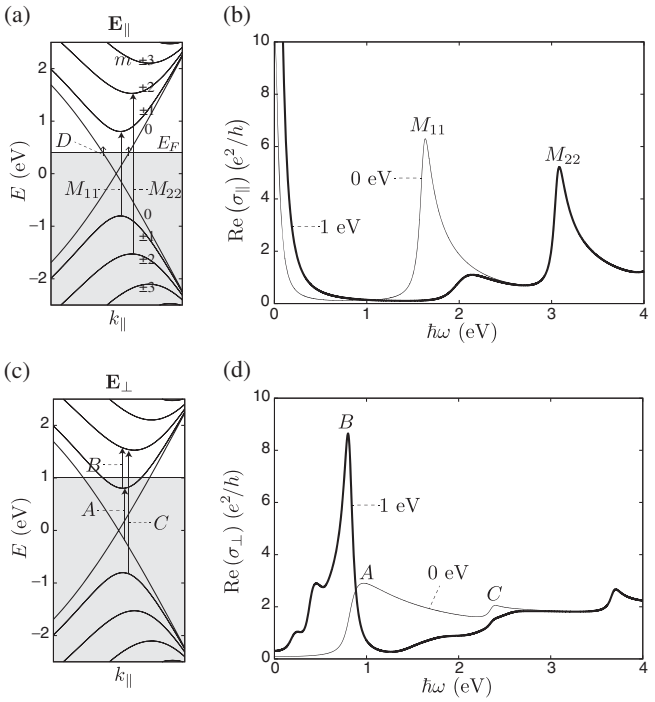

FIG. 2. Selection rule of armchair CNTs. (a) The direct transitions caused by $\mathbf{E}_\parallel$ ($\Delta m = 0$) are denoted by arrows. (b) Calculated real part of the dynamical conductivity along $\mathbf{E}_\parallel$, $\mathrm{Re}(\sigma_\parallel)$, is shown for different Fermi-energy positions. The vertical axis is given in units of e^2/h, where e is the electron charge magnitude and h is the Planck constant. (c) The momentum selection rule of $\mathbf{E}_\perp$ is $\Delta m = \pm 1$. The interband transitions with $m = 0 \to \pm 1$ are denoted by A, and these are allowed (forbidden) for low (high) doping. When $E_F = 1$ eV, the intraband transitions with $m = +1 \to +2$ or $-1 \to -2$ are allowed, and these are denoted by B. The transition C is suppressed by the pseudospin. (d) $\mathrm{Re}(\sigma_\perp)$ is shown for different Fermi-energy positions.

B. Perpendicular polarization

The electronic transition caused by $\mathbf{E}_\perp$ is the indirect transition, and transitions with an m change of ± 1, $\Delta m = \pm 1$, are dominant over transitions with $|\Delta m| \geq 2$. This selection rule is a consequence of momentum conservation being applied to a case where at the surface of a CNT, the azimuthal component of $\mathbf{E}_\perp$ is approximately written as a sine (or cosine) function of the azimuthal angle (θ) of the cylinder [2]. More precisely, this selection rule is a consequence of momentum conservation being used in combination with the two facts that a plane wave is a superposition of different magnetic quantum numbers and that tube diameter d_t of nanometer scale is much shorter than the light wavelength of micrometer scale [7,17]. The proof goes as follows. When the light polarization is set perpendicular ($\mathbf{e}_x$) to a tube's axis ($\mathbf{e}_z$), an incident plane wave of frequency ω and amplitude E_{in} is written as $E_{\mathrm{in}} e^{i(ky-\omega t)} \mathbf{e}_x$. In a cylindrical coordinate system (r, θ, z), the field is expressed as

$$\mathbf{E}_\perp(r, \theta; t) = E_{\mathrm{in}} e^{i(kr\sin\theta - \omega t)} \begin{pmatrix} \cos\theta \\ -\sin\theta \\ 0 \end{pmatrix}. \quad (1)$$

By using the formula for the Bessel functions $e^{ikr\sin\theta} = \sum_{m=-\infty}^{\infty} J_m(kr) e^{im\theta}$, we obtain the azimuthal component as

$$E_\theta = \sum_m \frac{E_{\mathrm{in}}}{2i} [J_{m+1}(kr) - J_{m-1}(kr)] e^{i(m\theta - \omega t)}. \quad (2)$$

Because $J_n(kr) \propto (kr)^n$, $|E_\theta|$ is dominated by the modes with $m = \pm 1$ when $kr \ll 1$, which we assume throughout this paper [18]. Applying the momentum selection rule to the band diagram in Fig. 2(c), we can expect that the transitions denoted by A and B to develop the peaks in $\mathrm{Re}(\sigma_\perp)$ for an undoped and doped CNT, respectively, and these are confirmed in Fig. 2(d).

The selection rule $\Delta m = \pm 1$ explained above is a result of the momentum conservation only, and the indirect transitions are further restricted to the forward scattering by the symmetry that originates from the two sublattice nature of the electronic wave function known as the pseudospin [20]. For example, it suppresses a transition

(of the backward scattering) denoted by C in Fig. 2(c) to develop a strong peak in $\mathrm{Re}(\sigma_\perp)$ like the M_{11} and M_{22} peaks, although it is a transition between band edges with a large density of states. A profound effect of the pseudospin on the selection rule is more clearly seen for a doped semiconducting CNT. In the band diagram of a (16,0) zigzag CNT shown in Fig. 3(a), each of the band curves is specified by shifted magnetic quantum number $m = \pm m_0 + n$, where m_0 is a nonzero integer ($m_0 = 11$) and $n = 0, \pm 1, \ldots$. When $E_F = 0.4$ eV, the transition denoted by C with $\Delta m = 1$ is allowed by the momentum selection rule; however, it is actually forbidden by the pseudospin. Meanwhile, the transition denoted by B with $\Delta m = -1$ is fully allowed. This difference is peculiar because the transition energy of C is smaller than that of B. It becomes clear that B (C) is forward (backward) scattering by drawing the three-dimensional band diagram in the inset of Fig. 3(b). As a result of the pseudospin, the peak position in $\mathrm{Re}(\sigma_\perp)$ is approximately given by 0.8 eV. The peak position of the doped zigzag CNT is similar to that of the doped armchair CNT [B in Fig. 2(d)], regardless of the difference of the band diagrams of the zigzag and armchair CNTs. It should be noted that the lack of the transition C with $\Delta m = 1$ does not mean that there is an asymmetry between the clockwise and anticlockwise circumferential motions of the electrons. Each band with the index n is actually degenerate ($\pm m_0$) corresponding to the different valleys, and the subband with n in one valley relates with the subband with $-n$ in the other valley. Thus, the lack of the transitions with $\Delta m = 1$ in one valley means the transitions with $\Delta m = 1$ in different valley are allowed.

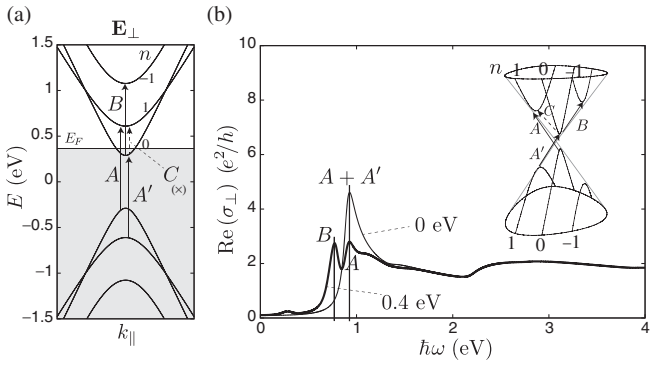

FIG. 3. Selection rule of zigzag CNTs. (a) The interband transitions denoted by A and A' are allowed when $E_F = 0$ eV. Because A and A' are forward scattering, a single peak develops in $\mathrm{Re}(\sigma_\perp)$ as shown in (b). When $E_F = 0.4$ eV, the peak intensity halves because A' is not allowed by the exclusion principle, whereas A is still allowed. In addition, the intraband transition B is allowed by the pseudospin. The three-dimensional band diagram shows that the transitions A, A', and B are all forward scattering, while C is backward scattering that is forbidden by the pseudospin.

III. DEPOLARIZATION AND THE PLASMON

According to the selection rule only, we may expect the peaks caused by $\mathbf{E}_\perp$, such as A in Fig. 2(d) and $A + A'$ in Fig. 3(b), to appear in the absorption spectra of undoped CNTs [21]. However, they do not. The calculated absorption spectrum, which is given by $\sigma_\perp$ divided by the relative permittivity $\varepsilon_\perp$ as $\mathrm{Re}(\sigma_\perp/\varepsilon_\perp)$ [$\equiv \mathrm{Re}(\tilde{\sigma}_\perp)$], does not exhibit the corresponding peak when $E_F = 0$ eV, as shown in the inset of Fig. 4. This is widely known as the depolarization effect [2–4]. As a result of the momentum transfer from $\mathbf{E}_\perp$ to an electron, a nonuniform density distribution around the tube's axis similar to an electric dipole is introduced and induces a depolarization field [2]. When the doping level is low, the depolarization field almost cancels out the applied field, and the total field defined by the sum of the applied and depolarization fields is suppressed. Even though the electronic transition is allowed by the selection rule, the electron does not undergo a transition since the electric field by itself almost disappears due to the depolarization effect.

The main point of this paper is that the efficacy of the depolarization field depends strongly on doping. When the doping level is as high as $E_F = 1$ eV, absorption peaks develop in the region near $\hbar\omega = 1.2$ eV as shown in Fig. 4. It can be shown that these peaks originate from the fact that the depolarization field is strongly enhanced at the specific frequency. Even if an infinitely small electric field is applied to a doped CNT, the depolarization field has a finite amplitude. This state is produced by the self-sustaining collective motion of the electrons (plasmon or plasmon polariton), which is in sharp

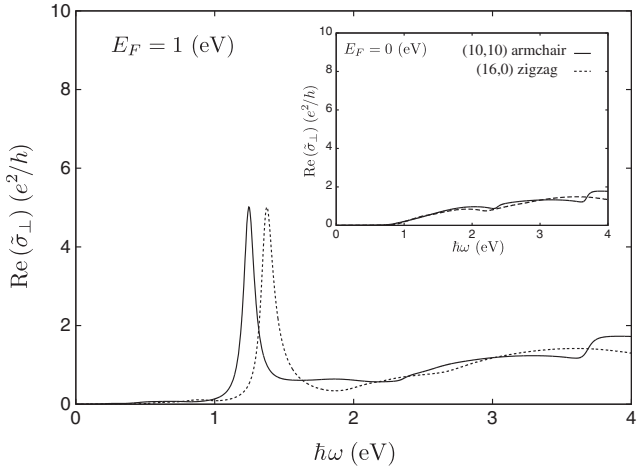

FIG. 4. Calculated absorption spectra for doped armchair and zigzag CNTs. The absorption spectrum that includes the depolarization effect is given by the real part of the dynamical conductivity divided by the relative permittivity $\varepsilon_\perp$, $\mathrm{Re}(\sigma_\perp/\varepsilon_\perp)$ [$\equiv \mathrm{Re}(\tilde{\sigma}_\perp)$]. The peak originates from a resonant excitation of the plasmon caused by doping. The inset shows the depolarization effect in undoped CNTs.

contrast to the single-particle excitation constituting the absorption peaks of $\mathbf{E}_{\parallel}$. Meanwhile, the Drude peak is absent for $\mathbf{E}_{\perp}$, which is also in contrast to the case of $\mathbf{E}_{\parallel}$.

The total electric field that the electrons in a CNT really "see" is given by the applied field divided by the relative permittivity $\mathbf{E}_{\perp}/\varepsilon_{\perp}$. Mathematically, it is shown that by solving Maxwell equations while taking account of the boundary conditions at the tube's surface [7], $\varepsilon_{\perp}$ is written as

$$\varepsilon_{\perp} = 1 - \frac{\sigma_{\perp}(E_F)}{i\omega\epsilon d_t}, \tag{3}$$

where d_t is the diameter of a CNT, and ϵ is the permittivity of the surrounding medium [2]. To observe that the vanishing real part of $\varepsilon_{\perp}$ is essential for the appearance of plasmon, we plot the real and imaginary parts of $\varepsilon_{\perp}$ as a function of energy in Fig. 5(a) for undoped and doped CNTs. Indeed, when $E_F = 1$ eV, $\mathrm{Re}(\varepsilon_{\perp})$ vanishes at an energy that corresponds to the absorption peak position seen in Fig. 4, where a small magnitude of $\mathrm{Im}(\varepsilon_{\perp})$ helps the total electric field to enhance in a resonant fashion. Note that in the present calculations, a surrounding medium with $\epsilon = 2\epsilon_0$ is assumed [12] where ϵ_0 is the permittivity of free space, and that a large value of ϵ/ϵ_0 has the advantage of decreasing the plasmon energy because $\mathrm{Re}(\varepsilon_{\perp})$ shifts upward in effect and zero of which shows a redshift.

To understand the cause of the appearance of plasmons in the doped CNTs more clearly, we consider the relative significance of the contributions made by intra- and interband transitions to $\mathrm{Re}(\varepsilon_{\perp})$ [17]. By noting that in Eq. (3), $\mathrm{Re}(\varepsilon_{\perp})$ is proportional to the imaginary part of the dynamical conductivity $\mathrm{Im}(\sigma_{\perp})$, we show each contribution $\mathrm{Im}(\sigma_{\perp}^{\mathrm{intra}})$ and $\mathrm{Im}(\sigma_{\perp}^{\mathrm{inter}})$ for the representative case of high doping level ($E_F = 1$ eV) in Fig. 5(b). $\mathrm{Im}(\sigma_{\perp}^{\mathrm{inter}})$ is a negative value for the frequency range of interest. Thus, if we neglect the intraband transitions, $\mathrm{Re}(\varepsilon_{\perp}) > 0$ and the condition for plasmon existence is unsatisfied. When $E_F = 1$ eV, the contribution made by the intraband transition (B) causes a peak in $\mathrm{Im}(\sigma_{\perp}^{\mathrm{intra}})$ so that $\mathrm{Re}(\varepsilon_{\perp})$ exhibits a dip at $\hbar\omega \approx 0.8$ eV. With increasing $\hbar\omega$ from a dip, $\mathrm{Im}(\sigma_{\perp}^{\mathrm{intra}})$ decreases and $-\mathrm{Im}(\sigma_{\perp}^{\mathrm{inter}})$ increases. As a result,

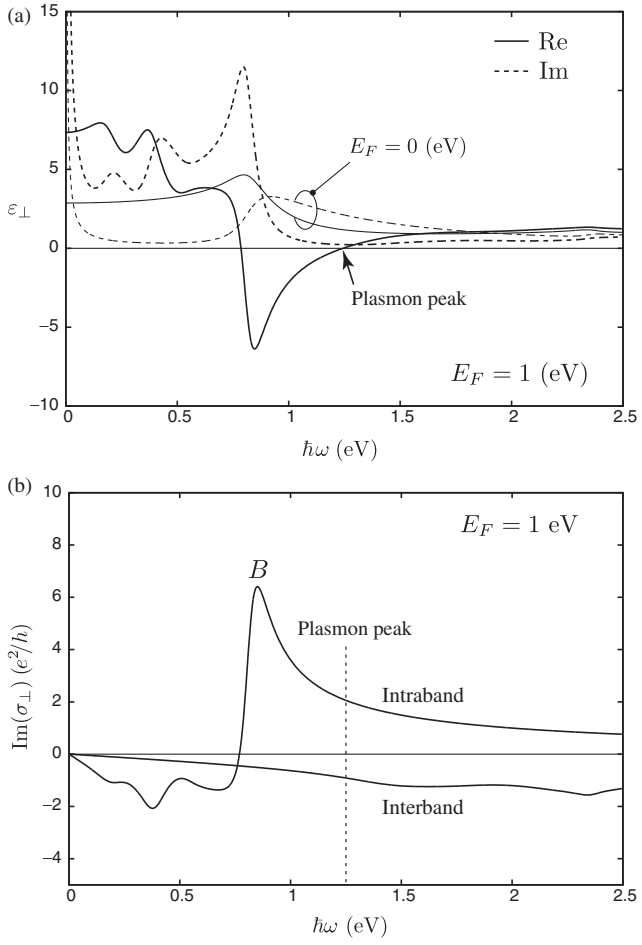

FIG. 5. Permittivity of $(10, 10)$ armchair CNTs. (a) $\mathrm{Re}(\varepsilon_{\perp})$ [$\mathrm{Im}(\varepsilon_{\perp})$] when $E_F = 1$ eV is shown by the solid (dashed) curve. The results when $E_F = 0$ eV are shown as a reference. (b) The intraband transitions caused by high doping are essential in the appearance of a plasmon peak. Meanwhile, the contribution of interband transitions is not negligibly small.

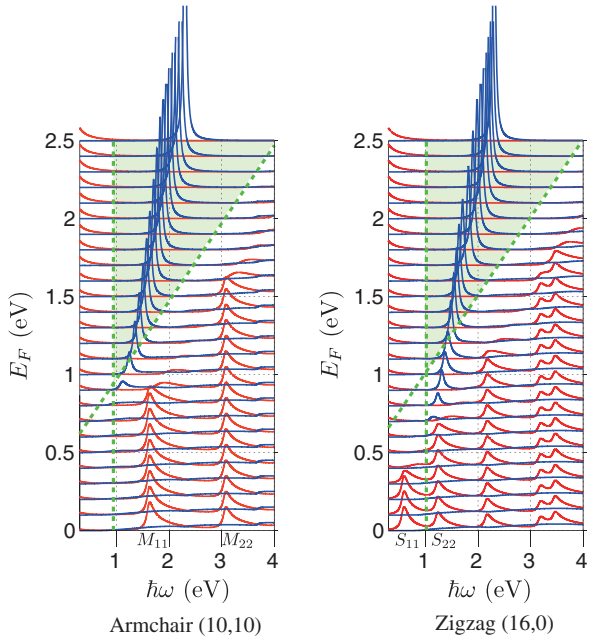

FIG. 6. Doping dependences of absorption spectra. Red (blue) spectra show the absorption of $\mathbf{E}_{\parallel}$ ($\mathbf{E}_{\perp}$). From the change in color of the absorption peak, it is clear that the polarization dependence of the peak is reversed by doping. Doping with $E_F \approx 1$ eV creates a transient region where the polarization anisotropy starts to be reversed. The green dotted line shows the boundary of single-particle excitation, and the green area ($\hbar\omega > 2\hbar v/d_t$ and $\hbar\omega < 2|E_F| - 2\hbar v/d_t$ where v is the Fermi velocity) shows the region where single-particle excitation does not exist [22].

$\mathrm{Re}(\varepsilon_\perp)$ becomes zero at around 1.2 eV, and the sign of $\mathrm{Re}(\varepsilon_\perp)$ changes at the energy. It is interesting that when combined with the intraband transitions, the contribution of the interband transitions to the dynamical conductivity is not negligible since it tends to redshift the plasmon energy when $E_F = 1$ eV.

Figure 6 shows the details of the E_F dependence of the absorption spectra of a (10,10) armchair ($d_t = 1.35$ nm) and (16,0) zigzag CNTs ($d_t = 1.25$ nm). There are several noticeable features that should be mentioned. First, the plasmon peak starts to develop when the M_{11} (S_{22}) peak by $\mathbf{E}_\parallel$ starts to disappear for the armchair (zigzag) CNT. Second, the plasmon peak intensity and frequency increase as E_F increases. Third, the doping dependence of the plasmon frequency in the armchair CNT is similar to that in the zigzag CNT. This suggests that when CNTs are intentionally doped, they will eventually have a similar excitation structure regardless of the chirality. Finally, the plasmon peak is present in the dispersion region (or the vicinity thereof) where single-particle excitation is not allowed, indicating that a plasmon cannot collapse into individual electron-hole pairs, and the kinematic stability is guaranteed for the plasmon.

IV. COULOMB INTERACTION

In this section, we examine how the Coulomb interaction affects the results presented in the preceding sections. Because the Coulomb interaction weakens at high doping or in a metallic CNT due to the screening effect, we focus on a semiconducting CNT at low doping level. The results shown in this section are obtained by extending the existing framework developed for calculating the exciton of an undoped CNT [23,24] to a doped CNT. The details are presented elsewhere [25].

The Coulomb interaction changes the absorption spectrum through two main effects: the self-energy correction to the band diagram (band renormalization) and the formation of excitons. First, we show the band renormalization.

A. Band renormalization

The thick curved lines in Fig. 7 show the renormalized band diagram of a (16,0) zigzag CNT, which is given by adding the screened exchange energy (or self-energy) to the original (bare) band diagram denoted by the thin curved lines. When $E_F = 0$ eV, the self-energy makes the band gap increase significantly. When $E_F = 0.5$ eV, on the other hand, the self-energy is modest; the band gap is almost identical to that of the bare band. This is because the electron-hole pairs within the conduction band screen the Coulomb interaction more effectively than the interband electron-hole pairs [22]. Note also that the self-energy for the states away from the Fermi level does not vanish, and this tends to blueshift the plasmon peak.

B. Absorption spectra

The exciton formation together with the band renormalization changes the absorption spectrum significantly. When $E_F = 0$ eV, the absorption peaks of $\mathbf{E}_\parallel$ are governed by excitons as shown in Fig. 8. By comparing the result with the spectrum calculated without the Coulomb interaction, the sizable enhancement of oscillator strength is seen for each peak. Meanwhile, the correction to the absorption spectrum of $\mathbf{E}_\perp$ is minor: a small peak due to the exciton formation is observed in $\mathrm{Re}(\tilde{\sigma}_\perp)$. These results are consistent with Refs. [23,24].

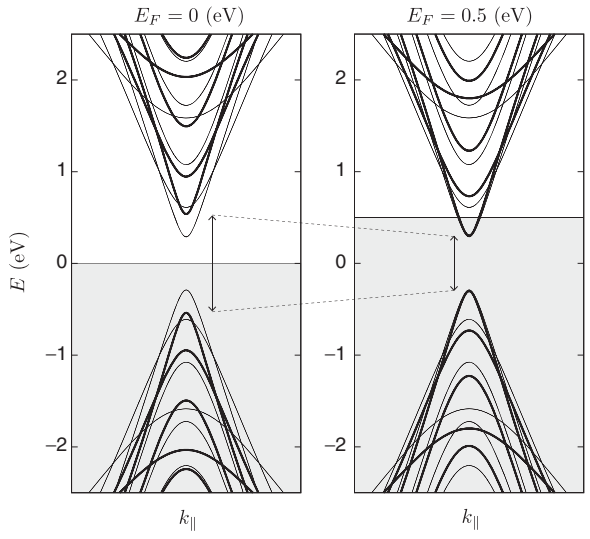

FIG. 7. Band renormalization of zigzag CNTs. Thick (thin) curved lines represent the renormalized (bare) band. The self-energy of the lowest-energy subbands is removed by modest doping ($E_F = 0.5$ eV) so that the band gap decreases.

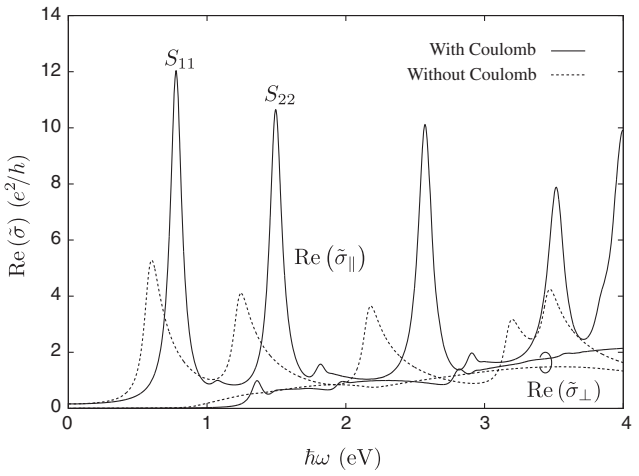

FIG. 8. Absorption spectra calculated with and without Coulomb interaction. $\mathrm{Re}(\tilde{\sigma}_\parallel)$ and $\mathrm{Re}(\tilde{\sigma}_\perp)$ of (16,0) undoped CNTs are shown.

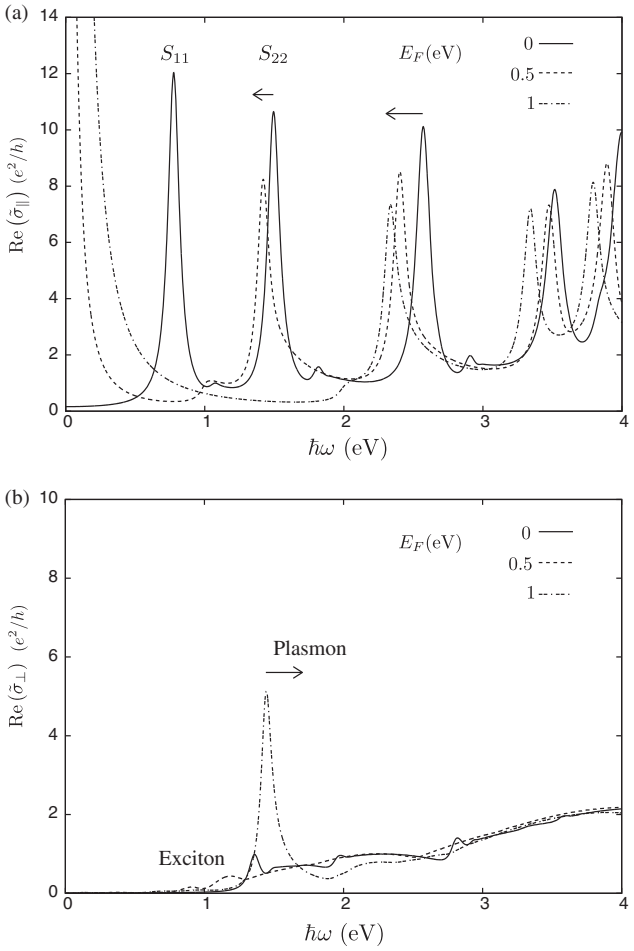

FIG. 9. Doping dependence of absorption spectra with Coulomb interaction. (a) When $E_F = 0.5$ eV, the S_{11} peak is invisible due to the exclusion principle, and the doping dependence of the S_{22} peak exhibits a redshift as indicated by the horizontal arrow. (b) The small exciton peak when $E_F = 0$ eV is replaced by a plasmon peak when $E_F = 1$ eV. This transition may be observed when the exciton peak is observable. The arrow above the plasmon peak shows that the plasmon energy increases with increased doping.

Figure 9(a) shows the behavior of the absorption peaks of $\mathbf{E}_{\parallel}$ under doping. When $E_F = 0.5$ eV, the S_{11} peak disappears due to the exclusion principle. The peak intensity of S_{22} (S_{33}) is suppressed by doping [9]. The further increase of doping results in the S_{22} and S_{33} peaks exhibiting redshift due to the band renormalization. The redshift of the peaks serves as a unique information of the self-energy because the peak positions should not change when the self-energy correction is not taken into account (see Fig. 6). As shown in Fig. 9(b), the exciton peak of $\mathbf{E}_{\perp}$ disappears soon after E_F reaches the bottom of the first subband ($E_F = 0.5$ eV), and the plasmon peak develops when $E_F = 1$ eV. Such a transition from exciton to plasmon may be observed when the broadening of the exciton of an undoped CNT is sufficiently suppressed [24].

V. DISCUSSION

We compare the present results with the experimental ones. Kazaoui *et al.* found a broad peak in the absorption by thin films of heavily doped single-walled CNTs [9]. The pristine films consist of semiconducting and metallic CNTs since S_{11} (0.68 eV), S_{22} (1.2 eV), and M_{11} (1.8 eV) are all observed. The doping-induced peak appears when S_{11}, S_{22}, and M_{11} disappear by doping, which is consistent with our results. It was found that the peak energy depends on the doping level: 1.07 eV (1.3 eV) for $CBr_{0.15}$ ($CCs_{0.10}$), while the details about the dependence was unknown. Igarashi *et al.* clarified that using electrochemical doping, the peak energy increases with increased doping [12]. They showed further that semiconducting and metallic single-walled CNTs cause independently the absorption peak at approximately 1 eV. These are consistent with our results. However, the calculated peak energy is slightly above (approximately 0.1 eV) the experimental result. This discrepancy warrants further examination. Petit *et al.* showed that doping thin films with naphthalene lithium did not cause the corresponding absorption peak even though the doping level is high enough to make an absorption peak [15]. This suggests an interesting possibility that the surrounding of CNTs is modulated by the doping and that doping has an influence on the plasmon absorption (such as the peak energy and intensity) through a mechanism beyond the description by static dielectric constant.

When fully verifying the proposed theory, it is desirable to orient CNTs that are doped and separated into a single chirality. In the past, the depolarization effect was experimentally verified by absorption and Raman spectroscopy in which undoped CNTs are oriented by stretching the organic films on which they are dispersed [4] or by controlling magnetic effects [26] or CNT growth processes [27]. Although experiments have already been performed on the doping dependence of light absorption for CNTs with a single chirality [12], there are no corresponding absorption measurements for oriented and doped CNTs. Recently, He *et al.* developed a technology for aligning CNTs spontaneously by improving vacuum filtration [28], and this approach can be used for the purpose.

If doped CNTs can be oriented, they will provide an opportunity for searching for novel phenomena even if they are not separated into a single chirality. Because the anisotropy of light absorption is related to the anisotropy of the electron-phonon interaction, there is a strong possibility that characteristic signals of doping will be explored by the polarized Raman spectroscopy [29]. For example, in doped metallic CNTs, phonon frequency hardening has been observed in the manner that depends on the phonon eigenvector [30]. A phenomenon similar to it should be observed also for semiconducting CNTs.

The idea of the polarization reversal of light absorption in doped CNTs can also be applied to doped graphene nanoribbons because it has been shown that the optical

selection rule of nanoribbons is similar to that of CNTs [20]. However, a modification of Eq. (3) caused by the edge is needed for nanoribbons, and the coupling of nanoribbons to the substrate must be taken into account.

Since the length of a CNT is finite in the axial direction, there is also a depolarization effect in the axial direction [31]. The optical selection rule of finite-length CNTs is obtained by extending the calculations on a nanoribbon. Indeed, due to the formation of a standing wave by the ends of a CNT, it can be proved that there is a wavelength shift of roughly the reciprocal of the axial length, which can explain why the plasmon peak is formed in the terahertz region of $\mathbf{E}_{\parallel}$ [31].

Here, we mention a subject closely related to the optical properties of doped CNTs, that is, quantum wells. The band diagram of a CNT bears a similarity to that of a quantum well, and the concepts such as depolarization and exciton effects are used to understand the optical properties of quantum wells. The term "intersubband transitions" is commonly used to describe only the transitions within the conduction band of quantum wells [32]. This is a reasonable assumption when the width of doped quantum wells is approximately 10 nm or longer. For CNTs with diameter of the order of 1 nm, however, the interband transitions have very important effects on absorption spectrum for both undoped and doped cases. Note also that the pseudospin selection rule is a fundamental new point of CNTs, not seen in quantum wells.

Two degrees of freedom of the light polarization are utilized in modern optical transmission technology to double the amount of information transmitted simultaneously. For example, a light is propagated by associating its parallel polarization with pictorial information and perpendicular polarization with sound. Nanoscale materials that respond differently depending on polarization direction are advantageous for information manipulation in highly refined structures where light propagates, for example, as an extremely thin Polaroid film. The fact that the polarization direction of light transmitted through CNTs can be rotated by 90° simply by doping implies the possibility of performing further information manipulation by electric means. From the viewpoint of condensed matter physics, the doping-induced change in the phase of the excited states from excitons to plasmons is an intriguing topic. Our conclusion is, thus, to stimulate both fundamental research on CNTs and application research related to optical devices.

ACKNOWLEDGMENTS

The authors thank K. Yanagi and J. Kono for discussions. Y. T. was supported by CREST JST (JPMJCR15N2).

APPENDIX: METHOD

We employ a tight-binding model with the hopping integral $\gamma = 2.6$ eV and atomic distance $a_{\mathrm{CC}} = 1.42$ Å to calculate the band diagram and wave function of the π electrons in CNTs [13]. As a function of wave vector $\mathbf{k} = (k_x, k_y)$, the model Hamiltonian is written in the form of a 2×2 matrix:

$$H(\mathbf{k}) = -\gamma \begin{pmatrix} 0 & f(\mathbf{k}) \\ f(\mathbf{k})^* & 0 \end{pmatrix}. \tag{A1}$$

The off-diagonal element $f(\mathbf{k})$ is a complex number given by

$$f(\mathbf{k}) = e^{ik_y a_{\mathrm{CC}}} + 2e^{-i[(k_y a_{\mathrm{CC}})/2]} \cos\left(\frac{\sqrt{3}k_x a_{\mathrm{CC}}}{2}\right), \tag{A2}$$

and $f(\mathbf{k})^*$ denotes the complex conjugate of $f(\mathbf{k})$. By expressing the energy eigenvalue equation $H(\mathbf{k})|\phi^s_{\mathbf{k}}\rangle = \varepsilon^s_{\mathbf{k}}|\phi^s_{\mathbf{k}}\rangle$ in terms of the magnitude and phase of $f(\mathbf{k})$ as $f(\mathbf{k}) = |f(\mathbf{k})|e^{-i\Theta(\mathbf{k})}$, we obtain the energy eigenvalue and Bloch wave function as $\varepsilon^s_{\mathbf{k}} = -s\gamma|f(\mathbf{k})|$ and

$$|\phi^s_{\mathbf{k}}\rangle = \frac{1}{\sqrt{2}} \begin{pmatrix} e^{-i\Theta(\mathbf{k})} \\ s \end{pmatrix}, \tag{A3}$$

respectively. The band index $s = +1$ ($s = -1$) corresponds to the valence (conduction) band. The low-energy band diagram near the charge neutrality point $\varepsilon^s_{\mathbf{k}} \sim 0$ is given by a pair of double cones (known as the Dirac cones).

Because the interaction between the electron and light δH is given by the minimal substitution $k_i \to k_i - (e/\hbar)A_i$, the electric currents defined from $\delta H = J_i A_i$ are

$$J_i = -\frac{e}{\hbar}\frac{\partial H(\mathbf{k})}{\partial k_i} \quad (i = x, y). \tag{A4}$$

Putting Eqs. (A1) and (A2) into Eq. (A4), we have the following expressions of the current operators,

$$J_x = -ev\frac{2}{\sqrt{3}}\sin\left(\frac{\sqrt{3}k_x a_{\mathrm{CC}}}{2}\right) \begin{pmatrix} 0 & e^{-i[(k_y a_{\mathrm{CC}})/2]} \\ e^{+i[(k_y a_{\mathrm{CC}})/2]} & 0 \end{pmatrix}, \tag{A5}$$

$$J_y = -ev\frac{2}{3} \begin{pmatrix} 0 & -i\left[e^{ik_y a_{\mathrm{CC}}} - e^{-i[(k_y a_{\mathrm{CC}})/2]}\cos\left(\frac{\sqrt{3}k_x a_{\mathrm{CC}}}{2}\right)\right] \\ i\left[e^{-ik_y a_{\mathrm{CC}}} - e^{i[(k_y a_{\mathrm{CC}})/2]}\cos\left(\frac{\sqrt{3}k_x a_{\mathrm{CC}}}{2}\right)\right] & 0 \end{pmatrix}, \tag{A6}$$

where $v \equiv 3\gamma a_{\mathrm{CC}}/2\hbar$ is the Fermi velocity of graphene.

The wave vectors are quantized by the periodic boundary condition around and along the tube's axis [16]. For the case of armchair (n,n) CNTs, the quantized wave vectors are specified by two integers m and j as

$$k_y \frac{3a_{\mathrm{CC}}}{2} n = m\pi, \quad (m = -n+1, \ldots, n), \tag{A7}$$

$$k_x \frac{\sqrt{3}a_{\mathrm{CC}}}{2} 2L = j\pi, \quad (j = -L, \ldots, L). \tag{A8}$$

Note that $2\sqrt{3}a_{\mathrm{CC}}L$ is the CNT length, $3a_{\mathrm{CC}}n/\pi$ is the diameter, and the surface area of a CNT (S) is $3a_{\mathrm{CC}}n \times 2\sqrt{3}a_{\mathrm{CC}}L$. As a result of the axial length being longer than the diameter ($L \gg n$), the band diagram of a CNT is well described by the cross sections of the Dirac cone [see Fig. 3(b)]. We also note that the effect of orbital hybridization between π and σ due to the curvature of the azimuthal direction is negligible in this study. For the case of zigzag $(n,0)$ CNTs, the quantized wave vectors are specified by two integers m and j as

$$k_y \frac{3a_{\mathrm{CC}}}{2} 2L = j\pi, \quad (j = -L, \ldots, L), \tag{A9}$$

$$k_x \frac{\sqrt{3}a_{\mathrm{CC}}}{2} n = m\pi, \quad (m = -n+1, \ldots, n). \tag{A10}$$

Note that $6a_{\mathrm{CC}}L$ is the CNT length, $\sqrt{3}a_{\mathrm{CC}}n/\pi$ is the diameter, and the surface area of a CNT is the same as (n,n) CNTs.

We calculate the dynamical conductivity in the framework of the linear response theory,

$$\sigma_{\Delta m}(\omega, E_F) \equiv g_{\mathrm{spin}} \frac{\hbar}{iS} \sum_{s',s} \sum_{m,j} \frac{[f^{s'}_{m+\Delta m,j}(E_F) - f^{s}_{m,j}(E_F)]|\langle \phi^{s'}_{m+\Delta m,j}|J_i|\phi^{s}_{m,j}\rangle|^2}{(\varepsilon^{s'}_{m+\Delta m,j} - \varepsilon^{s}_{m,j})(\varepsilon^{s'}_{m+\Delta m,j} - \varepsilon^{s}_{m,j} + \hbar\omega + i\delta)}, \tag{A11}$$

where $g_{\mathrm{spin}} = 2$ is the spin degeneracy, $f^s_{\mathbf{k}}(E_F) = 1/(e^{(\varepsilon^s_{\mathbf{k}} - E_F)/kT} + 1)$ is the Fermi distribution function at room temperature ($kT = 1/38.6$ eV), and δ ($= \hbar/\tau$) is inversely proportional to the relaxation time of an excited electron. We fix $\delta = 50$ meV ($\tau \approx 13$ fs) in all calculations. For an armchair CNT, the current operator J_x (J_y) couples to $\mathbf{E}_\parallel$ ($\mathbf{E}_\perp$). Because of the momentum selection rule $\Delta m = 0$ for $\mathbf{E}_\parallel$, the absorption $J_x E_x$ is the product of

$$\sigma_0 \tag{A12}$$

and E_x^2, while for $\mathbf{E}_\perp$, the absorption $J_y E_y$ is the product of

$$\frac{1}{2}\left(\frac{\sigma_{+1}}{1 - \frac{\sigma_{+1}}{i\omega\epsilon d_t}} + \frac{\sigma_{-1}}{1 - \frac{\sigma_{-1}}{i\omega\epsilon d_t}}\right) \tag{A13}$$

and E_y^2. The factor $1/2$ in Eq. (A13) originates from the field decomposition of E_y into the pair $\Delta m = \pm 1$. Equations (A12) and (A13) are the exact definition of the absorption plotted in the main text as $\sigma_\parallel$ and $\tilde{\sigma}_\perp$, respectively. Note also that $\sigma_{+1} = \sigma_{-1} (\equiv \sigma_\perp)$ holds in the absence of the Aharonov-Bohm flux along the tubule axis.

It is instructive to evaluate the matrix element to show that only the forward scattering is allowed by the selection rule of the pseudospin. We take zigzag CNTs and focus on the transitions between band edges ($k_y = 0$). The matrix element of J_x is known from Eqs. (A3) and (A5) as

$$\langle \phi^{s'}_{m'}|J_x|\phi^{s}_{m}\rangle \propto 1 + ss' e^{i(\Theta' + \Theta)}. \tag{A14}$$

Thus, for the interband transitions ($ss' = -1$), the transitions satisfying $\Theta' + \Theta = \pi$, which are the forward scattering, have the largest matrix element squared. For the intraband transitions ($ss' = 1$), the transitions satisfying $\Theta' + \Theta = 0$, which are the forward scattering too, are allowed. The intraband backward scattering satisfies $\Theta' + \Theta = \pi$ and has a vanishing matrix element [22].

The polarization characteristics of the absorption spectrum have been investigated for incident light energies up to 6 eV [27]. The absorption peaks observed at 4.5 and 5.25 eV are found to exhibit different polarization dependences. The behavior is also reproduced by our calculation shown in Fig. 10, that is, peaks caused by $\mathbf{E}_\parallel$ and $\mathbf{E}_\perp$ appear approximately at 5 and 6 eV, respectively. The discrepancy

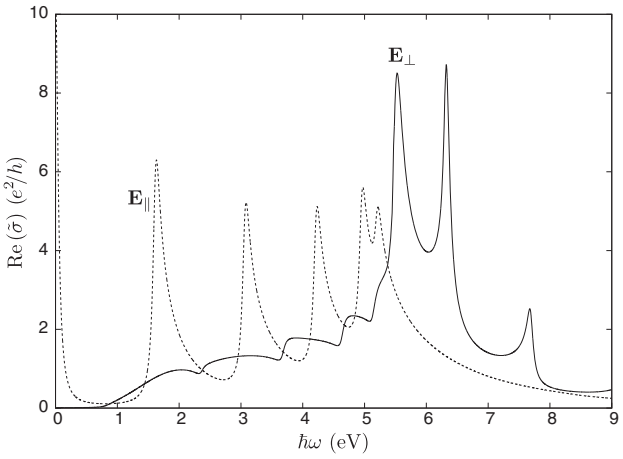

FIG. 10. Absorption spectra of $(10,10)$ armchair CNTs. The depolarization effect of $\mathbf{E}_\perp$ suppresses a peak to develop in $\mathrm{Re}(\tilde{\sigma}_\perp)$ at low energy ($\hbar\omega \approx 1$ eV). However, $\mathrm{Re}(\tilde{\sigma}_\perp)$ has the peaks at high energy around 6 eV.

between the experiment and calculation may be attributed to the fact that we ignore the overlap between the wave functions at nearest-neighbor π electrons giving asymmetry in the conduction and valence bands [13]. The qualitative agreement suggests the correctness of the optical matrix elements used to evaluate the dynamical conductivity. Note that the peak structure of $\mathrm{Re}(\tilde{\sigma}_{\perp})$ at about 6 eV may be regarded as a plasmon resonance because $\mathrm{Im}(\sigma_{\perp})$ has a peak structure at the energy and $\mathrm{Re}(\varepsilon_{\perp})$ approaches zero. Note also that a realistic doping level does not change these high-energy peaks and that the problem can be discussed simply in terms of the photoelectron interaction and the density of the electronic state [33].

[1] Sumio Iijima and Toshinari Ichihashi, Single-shell carbon nanotubes of 1-nm diameter, Nature (London) **363**, 603 (1993).

[2] Hiroshi Ajiki and Tsuneya Ando, Aharonov-Bohm effect in carbon nanotubes, Physica (Amsterdam) **201B**, 349 (1994).

[3] J. Hwang, H. H. Gommans, A. Ugawa, H. Tashiro, R. Haggenmueller, K. I. Winey, J. E. Fischer, D. B. Tanner, and A. G. Rinzler, Polarized spectroscopy of aligned single-wall carbon nanotubes, Phys. Rev. B **62**, R13310 (2000).

[4] M. Ichida, S. Mizuno, H. Kataura, Y. Achiba, and A. Nakamura, Anisotropic optical properties of mechanically aligned single-walled carbon nanotubes in polymer, Appl. Phys. A **78**, 1117 (2004).

[5] Satoru Shoji, Hidemasa Suzuki, Remo Proietti Zaccaria, Zouheir Sekkat, and Satoshi Kawata, Optical polarizer made of uniaxially aligned short single-wall carbon nanotubes embedded in a polymer film, Phys. Rev. B **77**, 153407 (2008).

[6] Byeong Gyun Kang, Young Jin Lim, Kwang-Un Jeong, Kyu Lee, Young Hee Lee, and Seung Hee Lee, A tunable carbon nanotube polarizer, Nanotechnology **21**, 405202 (2010).

[7] Ken-ichi Sasaki, Shuichi Murakami, and Hideki Yamamoto, Theory of intraband plasmons in doped carbon nanotubes: Rolled surface-plasmons of graphene, Appl. Phys. Lett. **108**, 163109 (2016).

[8] F. Javier García de Abajo, Graphene plasmonics: Challenges and opportunities, ACS Photonics **1**, 135 (2014).

[9] S. Kazaoui, N. Minami, R. Jacquemin, H. Kataura, and Y. Achiba, Amphoteric doping of single-wall carbon-nanotube thin films as probed by optical absorption spectroscopy, Phys. Rev. B **60**, 13339 (1999).

[10] X. Liu, T. Pichler, M. Knupfer, and J. Fink, Electronic and optical properties of alkali-metal-intercalated single-wall carbon nanotubes, Phys. Rev. B **67**, 125403 (2003).

[11] C. Kramberger, F. Roth, R. Schuster, R. Kraus, M. Knupfer, E. Einarsson, S. Maruyama, D. J. Mowbray, A. Rubio, and T. Pichler, Channeling of charge carrier plasmons in carbon nanotubes, Phys. Rev. B **85**, 085424 (2012).

[12] Toru Igarashi, Hideki Kawai, Kazuhiro Yanagi, Nguyen Thanh Cuong, Susumu Okada, and Thomas Pichler, Tuning Localized Transverse Surface Plasmon Resonance in Electricity-Selected Single-Wall Carbon Nanotubes by Electrochemical Doping, Phys. Rev. Lett. **114**, 176807 (2015).

[13] R. Saito, G. Dresselhaus, and M. S. Dresselhaus, *Physical Properties of Carbon Nanotubes* (Imperial College Press, London, 1998).

[14] E. D. Minot, Yuval Yaish, Vera Sazonova, and Paul L. McEuen, Determination of electron orbital magnetic moments in carbon nanotubes, Nature (London) **428**, 536 (2004).

[15] P. Petit, C. Mathis, C. Journet, and P. Bernier, Tuning and monitoring the electronic structure of carbon nanotubes, Chem. Phys. Lett. **305**, 370 (1999).

[16] Ermin Malić, Matthias Hirtschulz, Frank Milde, Andreas Knorr, and Stephanie Reich, Analytical approach to optical absorption in carbon nanotubes, Phys. Rev. B **74**, 195431 (2006).

[17] Craig F. Bohren and Donald R. Huffman, *Absorption and Scattering of Light by Small Particles* (Wiley, New York, 1983), ISBN 9780471293408.

[18] It is possible that in electron-energy-loss spectroscopy, the de Broglie wavelength may be comparable to d_t and electronic transitions satisfying $|\Delta m| \geq 2$ are allowed. Electronic transitions with $|\Delta m| = 2$ were demonstrated via Raman spectroscopy for an undoped CNT placed in a metal nanogap [19] where the light wavelength is reduced by the plasmon at the nanogap.

[19] Mai Takase, Hiroshi Ajiki, Yoshihiko Mizumoto, Keiichiro Komeda, Masanobu Nara, Hideki Nabika, Satoshi Yasuda, Hajime Ishihara, and Kei Murakoshi, Selection-rule breakdown in plasmon-induced electronic excitation of an isolated single-walled carbon nanotube, Nat. Photonics **7**, 550 (2013).

[20] Ken-ichi Sasaki, Keiko Kato, Yasuhiro Tokura, Katsuya Oguri, and Tetsuomi Sogawa, Theory of optical transitions in graphene nanoribbons, Phys. Rev. B **84**, 085458 (2011).

[21] I. Božović, N. Božović, and M. Damnjanović, Optical dichroism in nanotubes, Phys. Rev. B **62**, 6971 (2000).

[22] Ken-ichi Sasaki, Keiko Kato, Yasuhiro Tokura, Satoru Suzuki, and Tetsuomi Sogawa, Decay and frequency shift of both intervalley and intravalley phonons in graphene: Dirac-cone migration, Phys. Rev. B **86**, 201403 (2012).

[23] Tsuneya Ando, Excitons in carbon nanotubes, J. Phys. Soc. Jpn. **66**, 1066 (1997).

[24] Seiji Uryu and Tsuneya Ando, Exciton absorption of perpendicularly polarized light in carbon nanotubes, Phys. Rev. B **74**, 155411 (2006).

[25] The results shown in this section are dependent on an energy cutoff E_c which limits the electron or hole states being taken into account in evaluating the physical quantities. We set $E_c = \gamma$.

[26] M. F. Islam, D. E. Milkie, C. L. Kane, A. G. Yodh, and J. M. Kikkawa, Direct Measurement of the Polarized Optical Absorption Cross Section of Single-Wall Carbon Nanotubes, Phys. Rev. Lett. **93**, 037404 (2004).

[27] Yoichi Murakami, Erik Einarsson, Tadao Edamura, and Shigeo Maruyama, Polarization Dependence of the Optical Absorption of Single-Walled Carbon Nanotubes, Phys. Rev. Lett. **94**, 087402 (2005).

[28] Xiaowei He, Weilu Gao, Lijuan Xie, Bo Li, Qi Zhang, Sidong Lei, John M. Robinson, Erik H. Hároz, Stephen K. Doorn, Weipeng Wang, Robert Vajtai, Pulickel M. Ajayan, W. Wade Adams, Robert H. Hauge, and Junichiro Kono,

Wafer-scale monodomain films of spontaneously aligned single-walled carbon nanotubes, Nat. Nanotechnol. **11**, 633 (2016).

[29] Martin Kalbac, Hootan Farhat, Ladislav Kavan, Jing Kong, Ken-ichi Sasaki, Riichiro Saito, and Mildred S. Dresselhaus, Electrochemical charging of individual single-walled carbon nanotubes, ACS Nano **3**, 2320 (2009).

[30] H. Farhat, H. Son, Ge. G. Samsonidze, S. Reich, M. S. Dresselhaus, and J. Kong, Phonon Softening in Individual Metallic Carbon Nanotubes Due to the Kohn Anomaly, Phys. Rev. Lett. **99**, 145506 (2007).

[31] Qi Zhang, Erik H. Hároz, Zehua Jin, Lei Ren, Xuan Wang, Rolf S. Arvidson, Andreas Lüttge, and Junichiro Kono, Plasmonic nature of the terahertz conductivity peak in single-wall carbon nanotubes, Nano Lett. **13**, 5991 (2013).

[32] H. C. Liu and Federico Capasso, *Intersubband Transitions in Quantum Wells: Physics and Device Applications I* (Academic Press, New York, 2000), ISBN 9780080864600.

[33] F. L. Shyu and M. F. Lin, π plasmons in two-dimensional arrays of aligned carbon nanotubes, Phys. Rev. B **60**, 14434 (1999).